JOURNAL OF BACTERIOLOGY, Oct. 1992, p. 6527–6538
0021-9193/92/206527-12$02.00/0

Vol. 174, No. 20

The S-Layer of *Caulobacter crescentus*: Three-Dimensional Image Reconstruction and Structure Analysis by Electron Microscopy

JOHN SMIT,[1]* HARALD ENGELHARDT,[2] SUSANNE VOLKER,[2] STEPHEN H. SMITH,[1]† AND WOLFGANG BAUMEISTER[2]

Max-Planck-Institut für Biochemie, D-8033 Martinsreid bei Munich, Germany,[2] and Department of Microbiology, University of British Columbia, Vancouver, British Columbia V6T 1Z3, Canada[1]

Received 15 May 1992/Accepted 28 July 1992

The regular surface protein structure (S-layer) of *Caulobacter crescentus* was analyzed by electron microscopy and three-dimensional image reconstruction to a resolution of 2 nm. Projections showed that the S-layer is an array of ring structures, each composed of six subunits that are arranged on a lattice with p6 symmetry. Three-dimensional reconstructions showed that the ring subunits were approximately rod-shaped structures and were perpendicular to the plane of the array, with a linker arm emanating from approximately the middle of the rod, accounting for the connections between the rings. The calculated subunit mass was ca. 100 kDa, very close to the size of RsaA (the protein known to be at least the predominant species in the S-layer) predicted from the DNA sequence of the *rsaA* gene. The core region of the rings creates an open pore 2.5 to 3.5 nm in diameter. The size of the gaps between the neighboring unit cells is in the same range, suggesting a uniform porosity predicted to exclude molecules larger than ca. 17 kDa. Attempts to remove membrane material from S-layer preparations with detergents revealed that the structure spontaneously rearranged into a mirror-image double layer. Negative-stain and thin-section electron microscopy examination of colonies of *C. crescentus* strains with a mutation in a surface molecule involved in the attachment of the S-layer showed that shed RsaA protein organized into large sheets. The sheets in turn organized into stacks that tended to accumulate near the upper surface of the colony. Image reconstruction indicated that these sheets were also precise mirror-image double layers, and thickness measurements obtained from thin sections were consistent with this finding. The sheets were absent when these mutant strains were grown without calcium, supporting other data that calcium is involved in attachment of the S-layer to a surface molecule and perhaps in subunit-subunit interactions. We propose that when the membrane is removed from S-layer fragments by detergents or the attachment-related surface molecule is absent, the attachment sites of the S-layer align precisely to form a double layer via a calcium interaction.

Regularly arrayed surface layers composed of a single protein species (S-layers) are a feature found in many bacteria and form geometrically arranged two-dimensional structures on the outermost bacterial surface (4, 14, 25, 26). There is evidence that S-layers provide a protective barrier for cells that enables them to resist attack by lytic enzymes or by bdellovibrios (16) or possess key surface features that enable them to interact with host organisms to effect pathogenesis (3, 14, 15, 26). It seems reasonable that to be a protective barrier, an S-layer must completely cover a cell. This seems to be the case in *Caulobacter crescentus*; although significant morphogenesis occurs, the entire bacterium, including the stalk, is covered at all times (27, 29).

Three-dimensional (3D) reconstructions provide insight into the spatial organization of the S-layer proteins. When the domain structure can be correlated with the primary structure of the protein, it will be possible to describe the properties of the S-layer surface in more detail. This particularly applies to subunit-subunit interactions, to regions exposed to the environment, and to regions interacting with the underlying cell envelope components. Such a description is becoming possible for several species whose S-layer genes have been cloned and sequenced and for which the possibility for high-resolution image analysis exists (6, 7, 17, 18, 30, 31). *C. crescentus* is such a species. The protein of the S-layer has been isolated and characterized in several ways, and a two-dimensional image analysis of the paracrystalline structure has been done (29). A single-copy gene has been cloned for the protein and sequenced (12, 13, 28). Mutants that are capable of producing an S-layer structure but fail to attach the protein to the surface have been isolated, and a surface molecule that appears responsible for this interaction has been identified (9, 32). Finally, we have demonstrated that a *C. crescentus* bacteriophage uses the S-layer protein as a receptor for infection (9).

We now present a 3D reconstruction of the *C. crescentus* S-layer obtained from natural crystal patches. These patches still contained material originating from the outer membrane when prepared by methods described by Smit et al. (29) and were expected to have an impact on the resolving capability of image-averaging techniques. The S-layer-shedding mutants, on the other hand, produced large arrays of an assembled structure adjacent to cells when colonies of cells were gently suspended in preparation for electron microscopy analysis. These patches were well ordered and were frequently larger than the surface area of a single cell; on that basis, we presumed them to be in vitro assembly products of the S-layer protein. Such patches were free of membrane material. By exploring the suitability for 3D reconstructions of these patches, as well as S-layer fragments freed from

* Corresponding author.
† Present address: Department of Anatomy, University of British Columbia, Vancouver, British Columbia V6T 1Z3, Canada.

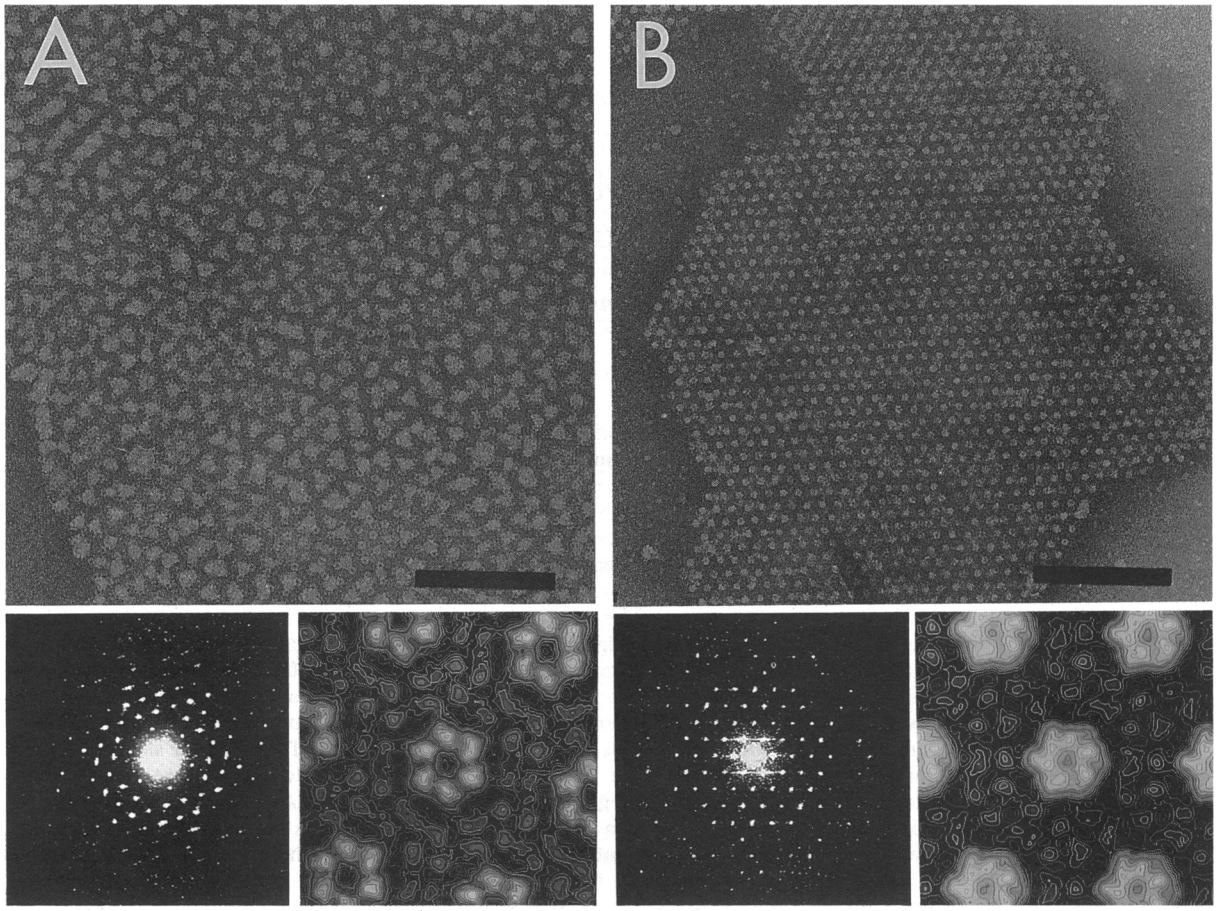

FIG. 1. S-layer preparations from *C. crescentus* CB15NY106 negatively stained with ammonium molybdate. (A) S-layer still associated with vesicles originating from the outer membrane. The corresponding power spectrum and the nonsymmetrized correlation average are displayed below. The resolution of the average is 2.2 nm (351 unit cells averaged), and the lattice spacing (center-to-center distance) is 22.0 nm. (B) S-layer treated with deoxycholate, apparently free of visible, attached membrane material. The corresponding power spectrum and the nonsymmetrized correlation average are displayed below. The resolution is 2.1 nm (406 unit cells averaged), and the center-to-center distance is 20.6 nm. Bars, 200 nm.

membrane material by detergents, we obtained valuable information about the means of S-layer attachment to the cell surface.

MATERIALS AND METHODS

Bacterial strains and growth conditions. Strains CB15NY106 and NA1000 were derived from *C. crescentus* CB15 (ATCC 19089); the former was used for the isolation of S-layer fragments (29), while the latter was a derivative from which synchronously growing cells were readily prepared. NA1000 was formerly referred to as CB15A and is probably the same as strains CB15N and CB15F described by other authors. CB15Ca5 and CB15Ca10 were spontaneous mutants of NA1000, selected for the ability to grow in the absence of calcium (9, 32). A coincident phenotype is that they are able to assemble RsaA, the protein that constitutes the *C. crescentus* S-layer, into a crystalline structure when grown in a calcium-containing medium but fail to attach the protein to the cell surface.

For most experiments, cells were grown in a peptone-yeast extract medium that was supplemented with 20 mM $MgCl_2$ and 10 mM $CaCl_2$ (PYE) (19) and that was solidified when appropriate with agar at 15 g/liter. M_3HiGG mineral salts medium (29) is a variation of the HiGG medium described by Poindexter (20) and was used for the production of S-layer fragments from CB15NY106. M_{10}HiGG is a calcium-free mineral salts medium (9) that was solidified with the addition of nucleic acid electrophoresis-grade agarose at 8 g/liter.

S-layer preparations. Fragments of a crystallized S-layer (with associated membrane material) were prepared by differential centrifugation of high-density cultures of CB15NY106 grown in M_3HiGG medium as previously described (29). To examine S-layer patches in experiments with S-layer-shedding mutants, we suspended colonies growing on PYE medium in 10 μl of water in preparation for negative staining.

Negative-stain electron microscopy and image reconstruction. The S-layer preparations or cell suspensions were adsorbed onto carbon-coated copper grids made hydrophilic by glow discharge. After the removal of excess material by wicking to filter paper, the specimens were negatively stained with 2% ammonium molybdate (pH 7.5). In some experiments, S-layer preparations were mixed with equal quantities of detergent solutions for several minutes before the negative-stain step. The detergent solutions included

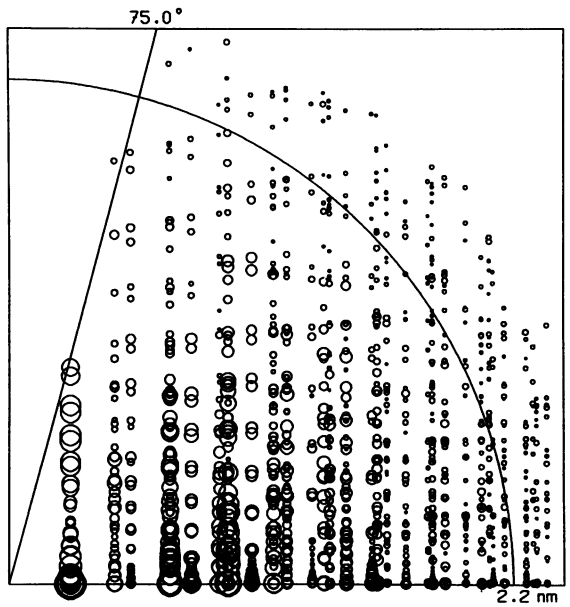

FIG. 2. Distribution of data in Fourier space. The ordinate represents spatial frequencies of the Fourier components sampled along the lattice lines, and the abscissa represents the distance of the lattice lines from the center of the Fourier transform. The area of each circle is proportional to the modulus of the corresponding Fourier component. The line demarcates the missing cone of data that remains after tilting to 75°. The curve corresponds to a resolution of 2.2 nm.

0.2% deoxycholate (pH 9.3), 2% octyl-polyoxyethylene, 0.1% sodium dodecyl sulfate, and 0.1% lithium dodecyl sulfate.

The preparations were inspected in a Philips EM420 or CM12 electron microscope, and micrographs were taken, usually under low-dose conditions. To reduce irradiation, we performed focusing and correction for astigmatism on areas close to the S-layer sheets to be recorded. The primary magnification was ×36,000 or ×39,000, respectively. Short tilt series consisting of three to five micrographs were taken in addition to complete series consisting of 15 projections recorded at tilt angles ranging from 0° to 75° to 80°, in accordance with the tilting scheme of Saxton et al. (24). Micrographs showing well-ordered crystals and optimum focus conditions in the light optical diffractometer were selected for densitometry and image-processing purposes. Areas of 1,024 by 1,024 pixels were digitized with an Eikonix 1412 camera system by applying a pixel size of 0.43 nm at the specimen level.

The images were averaged by applying correlation averaging as described by Saxton and Baumeister (22), and the averages were subjected to 3D reconstruction by the hybrid real space-Fourier space approach (24). Several reconstructions were performed with continuous tilt series as well as discontinuous tilt series consisting of individual projections from short tilt series. Resolutions were assessed on the basis of the radial correlation function criterion (22). For image-processing and reconstruction purposes, the SEMPER 6.2 system was used throughout (24a).

S-layer preparations from mutant strain *C. crescentus* CB15Ca5 were also embedded in aurothioglucose (ATG) by mixing equal amounts of cell suspensions and 4% ATG and applying the mixtures to grids. These were imaged under low-dose conditions in the CM12 electron microscope with an on-line image-processing system as described previously (21).

Thin-section electron microscopy of undisturbed colonies. Bacterial strains were grown at 30°C to a colony diameter of 1 to 1.5 mm on PYE or M_{10}HiGG (calcium-deficient) medium. Colonies were overlaid with homologous agar medium kept at a temperature just above the solidification point (ca. 50°C). The "sandwiched" colonies were excised, and the

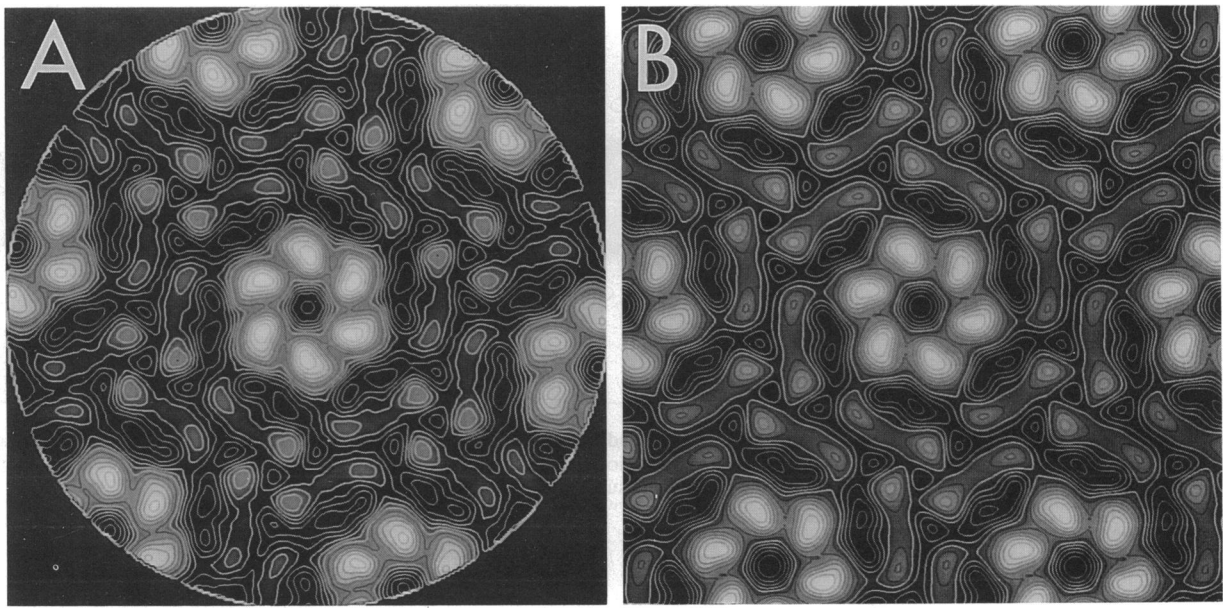

FIG. 3. Contoured images of the *C. crescentus* S-layer obtained from the sixfold-symmetrized average of the 0° tilt projection used for the 3D reconstruction (A) and the appropriate projection through the complete data set of the 3D reconstruction (B). The dimensions of each image are 44 by 44 nm.

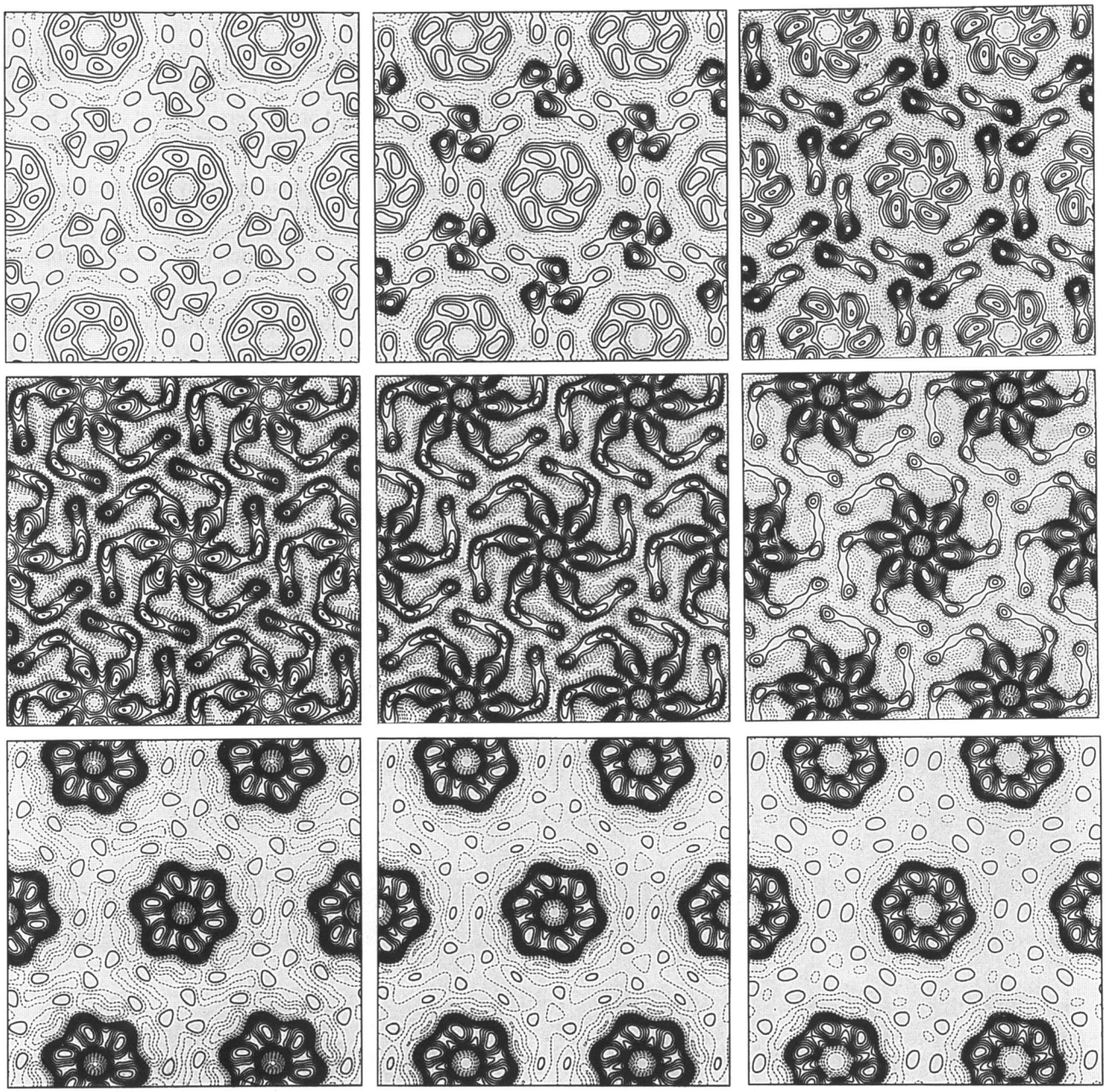

FIG. 4. Horizontal sections through the 3D reconstruction obtained from a complete, continuous tilt series, sampled at 0.15-nm spacings. The sections displayed are distant from each other by 0.6 nm. Horizontal sections through the 3D reconstruction obtained from the combination of four different short tilt series yielded very similar results (data not shown).

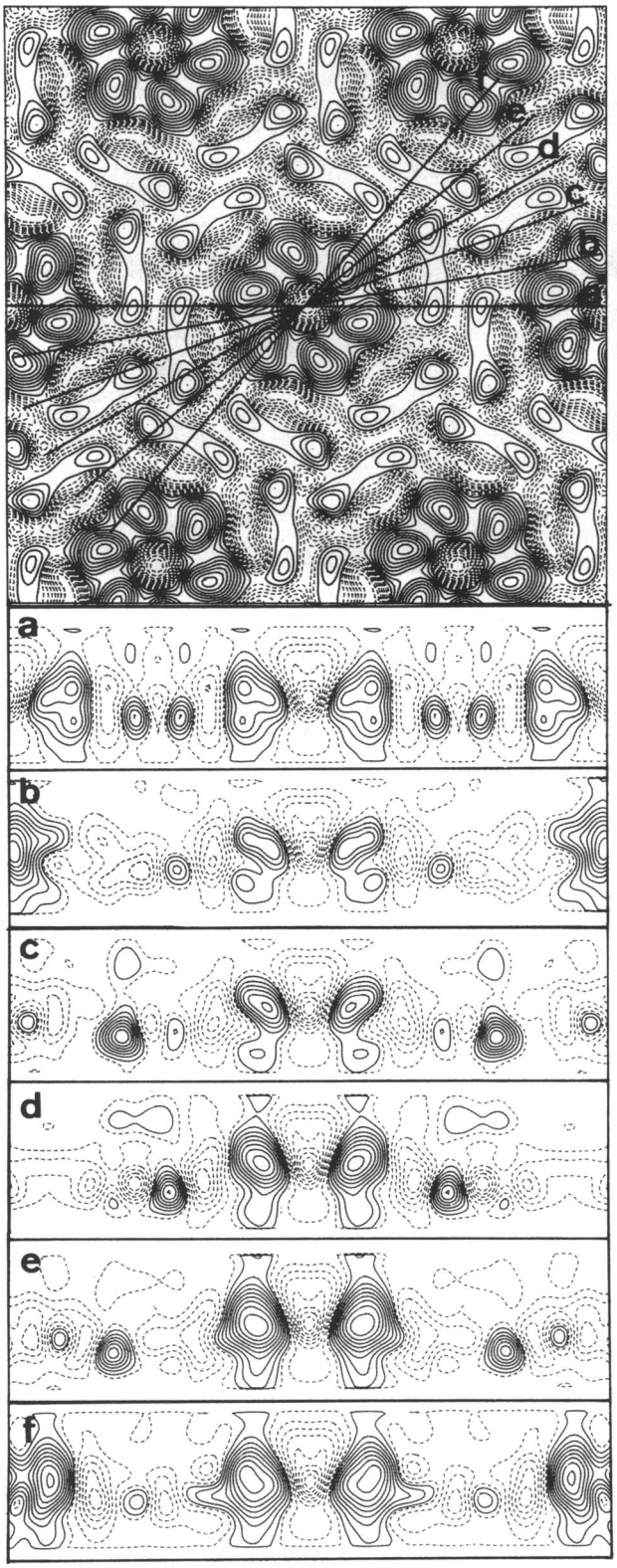

FIG. 5. Vertical sections through the 3D reconstruction. The upper panel shows the vertical projection, and the lines indicate the orientations of the vertical sections (a to f) displayed below. The size of each section is 44 by 12.3 nm.

blocks obtained were immersed in fixative (5% acrolein–0.25% glutaraldehyde in 50 mM sodium cacodylate buffer [pH 7.3]) overnight at 4°C. The blocks were rinsed in buffer and placed in 0.8% tannic acid in buffer for 45 min at room temperature. The blocks were rinsed again in buffer and postfixed with freshly prepared 1% osmium tetroxide–0.1% ruthenium red in buffer for 1 h at 4°C. After a distilled water rinse, the blocks were treated with saturated uranyl acetate for 1 h, dehydrated with a graded series of ethanol, and embedded in Spurr's resin. Thin sections were prepared and stained with uranyl acetate and Reynolds' lead citrate. Specimens were viewed in a Siemens 101A electron microscope operated at 80 kV.

RESULTS AND DISCUSSION

Negative-stain electron microscopy of the S-layer. The typical preparation of the S-layer isolated from *C. crescentus* CB15NY106 yields S-layer arrays still contaminated with what is likely to be fragments of the outer membrane (29). Figure 1A illustrates the typical appearance of an S-layer fragment, with the triangular membrane vesicles attached to the layer such that it is centered on a threefold symmetry axis. Three linker domains (arms), connecting three hexagons, as well as two core domains of each of the three neighboring hexagons are covered by the membrane material. Appropriate correlation averages illustrate the distribution of the lipid over the unit cell (data not shown). The triangular membrane vesicles are apparently irregularly distributed with respect to the lateral, as well as the angular, orientation. Correlation averages of the unit cells appeared not to be influenced by the attached lipid. This result was expected; the membrane material contributes to the mean value only and thus should remain invisible in the averaged images (Fig. 1A).

Some effort was made to remove the attached lipid. Octyl-polyoxyethylene treatment resulted in residual crystallized detergent that prevented proper negative staining of the S-layer. Sodium dodecyl sulfate and lithium dodecyl sulfate treatments tended to result in "rolled-up" S-layer patches, leading to multiple layers of the crystalline structure that were useless for image analysis. Treatment with deoxycholate for 1 to 2 min apparently freed the S-layer from the membrane vesicles but allowed the layer to remain intact and well ordered (Fig. 1B). Image analysis, however, revealed that a rearrangement had occurred; all the deoxycholate-treated sheets were double layers in all micrographs inspected. The two layers were nearly perfectly in register, such that moiré patterns could be detected only rarely (Fig. 1B). The averaged unit cells, however, consistently were less regular with respect to rotational symmetry than those obtained from the untreated S-layer preparations. It is quite possible that the double layers were not stained completely or that there was some lateral displacement of the second layer, due either to distortion during drying or to surface effects of the carbon support film. The latter would yield undisturbed reflections in the power spectra but clearly disturbed symmetry properties of the unit cell. The decline in regularity could also have been due to residual lipid still situated on the core and presumably in the pore, which appeared closed in the averaged image.

Since the resolutions were the same with both preparations, close to 2.1 nm each (Fig. 1), we chose the original preparations for reconstruction purposes.

Assessment of the 3D reconstruction data. Two strategies were applied to collect data for 3D reconstructions. We took

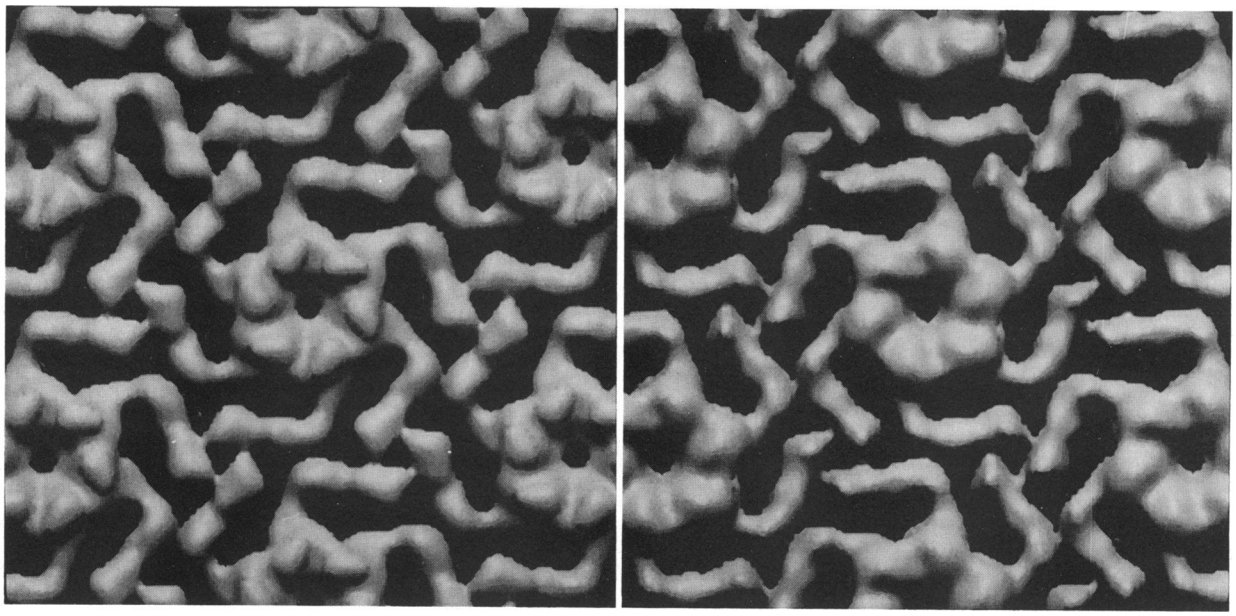

FIG. 6. Computer-generated views of the two surfaces of the 3D reconstruction of the *C. crescentus* S-layer.

several complete, continuous tilt series and a number of short tilt series consisting of three to five projections only. From the latter, appropriate averages were merged to form a complete 3D data set. The reconstructions comprised 14 projections each, and the tilt range was consistently 0° to 78°.

The distribution of the components in the Fourier space was homogeneous to a resolution of about 2 to 2.2 nm for both reconstructions. Only the lattice line 1,0 was significantly affected by the limited tilt range (Fig. 2). The two reconstructions were of comparable quality and yielded almost identical structures of the S-layer in the *xy* plane as well as in the *z* direction. Since the lattice lines of the continuous tilt series proved to be slightly more significant, mainly this reconstruction is documented here. The average of the 0° tilt projection and the appropriate projection through the complete 3D reconstruction illustrate the reliability of the reconstructed data (Fig. 3).

Description of the S-layer structure. The 0° tilt projection shows a clear handedness of the hexagonal core and the arms linking neighboring unit cells (Fig. 3). According to the classification scheme of Saxton and Baumeister (23), the layer is of type M_6C_3. This classification is also confirmed with the horizontal sections (Fig. 4), in which connectivity is seen to occur exclusively around the threefold symmetry axis. The putative monomer of the S-layer is an elongated and twisted molecule. The arms are connected close to one surface of the layer, but they proceed approximately to the center of the core with respect to the *z* direction, where they change over into the core region, forming the pore. The arms are therefore somewhat inclined, a feature uncommon to S-layers reconstructed so far. The vertical sections shown in Fig. 5 illustrate this fact more clearly.

The center-to-center distance between the core regions was calculated to be 22 nm, a refinement of the earlier estimate of 23.5 nm (29). The core region creates an open pore (Fig. 4 and 5) with a diameter of approximately 2.5 to 3.5 nm. The size of the gaps between the neighboring unit cells is in the same range. Thus, the S-layer may prevent the penetration of globular molecules larger than ca. 17 kDa.

The 3D models (Fig. 6) of both surfaces of the S-layer show quite similar surface views. This impression is mainly due to the fact that the arms are inserted near the center of the core.

The solid model represents a mass, calculated by a previously described method (10), of about 100 kDa for the monomer, a mass close to that of the mature protein, predicted from the translated sequence of the *C. crescentus* S-layer protein gene, *rsaA*, to be 98,001 kDa (13). This finding, along with the ability to recrystallize the S-layer from purified RsaA (33), unambiguously indicates that RsaA alone can account for all the visible elements of the *C. crescentus* S-layer.

The two 3D reconstructions performed, that is, the reconstructions of the continuous tilt series and of the merged projections, were essentially indistinguishable. They revealed the same architecture of the S-layer, with almost no differences in structural details. Minor deviations of structural features are insignificant with regard to the resolution of the reconstructions. The thicknesses of the two reconstructions are identical and are close to 7 nm. The similarity in thickness corroborates our experience with reconstructions of other S-layers. That is, the use of continuous tilt series of negatively stained preparations recorded under low-dose conditions (as is usually done) does not drastically reduce the thickness of the specimen by reason of prolonged electron irradiation. Clear examples are the reconstructions of the structurally very similar S-layers of *Azotobacter vinelandii* (5) and *Aeromonas hydrophila* (1), which differ by only 0.5 nm, i.e., 10%, in thickness. This difference may indeed be due to the effects of specimen tilting limitations (producing the "missing cone"; see references 2 and 10 for a discussion). The S-layer of *Deinococcus radiodurans* (the HPI layer) has a thickness of 6 nm in the 3D reconstruction of negatively stained preparations obtained from a continuous tilt series (3) as well as in the reconstruction of merged projections of preparations embedded in cadmium-thioglycerol under low-dose conditions (14a). Even determinations of thickness by means of scanning tunneling microscopy did

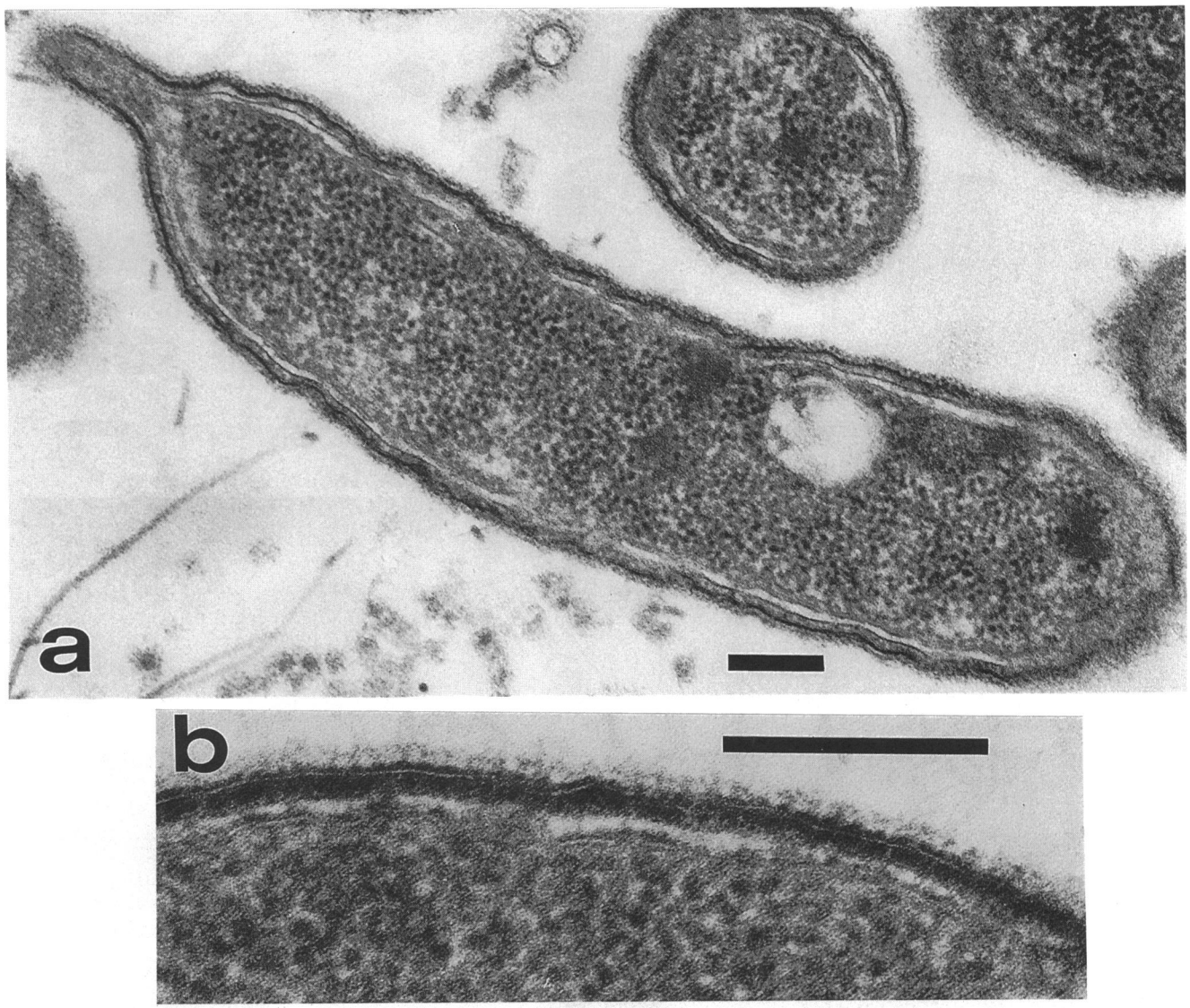

FIG. 7. Thin sectioning of *C. crescentus* NA1000 (wild-type S-layer). (a) Note the uniform, structured S-layer covering the entire surface of the cell, including the stalk. (b) Higher magnification of another cell, showing the repeat structure of the S-layer. Bars, 0.2 μm.

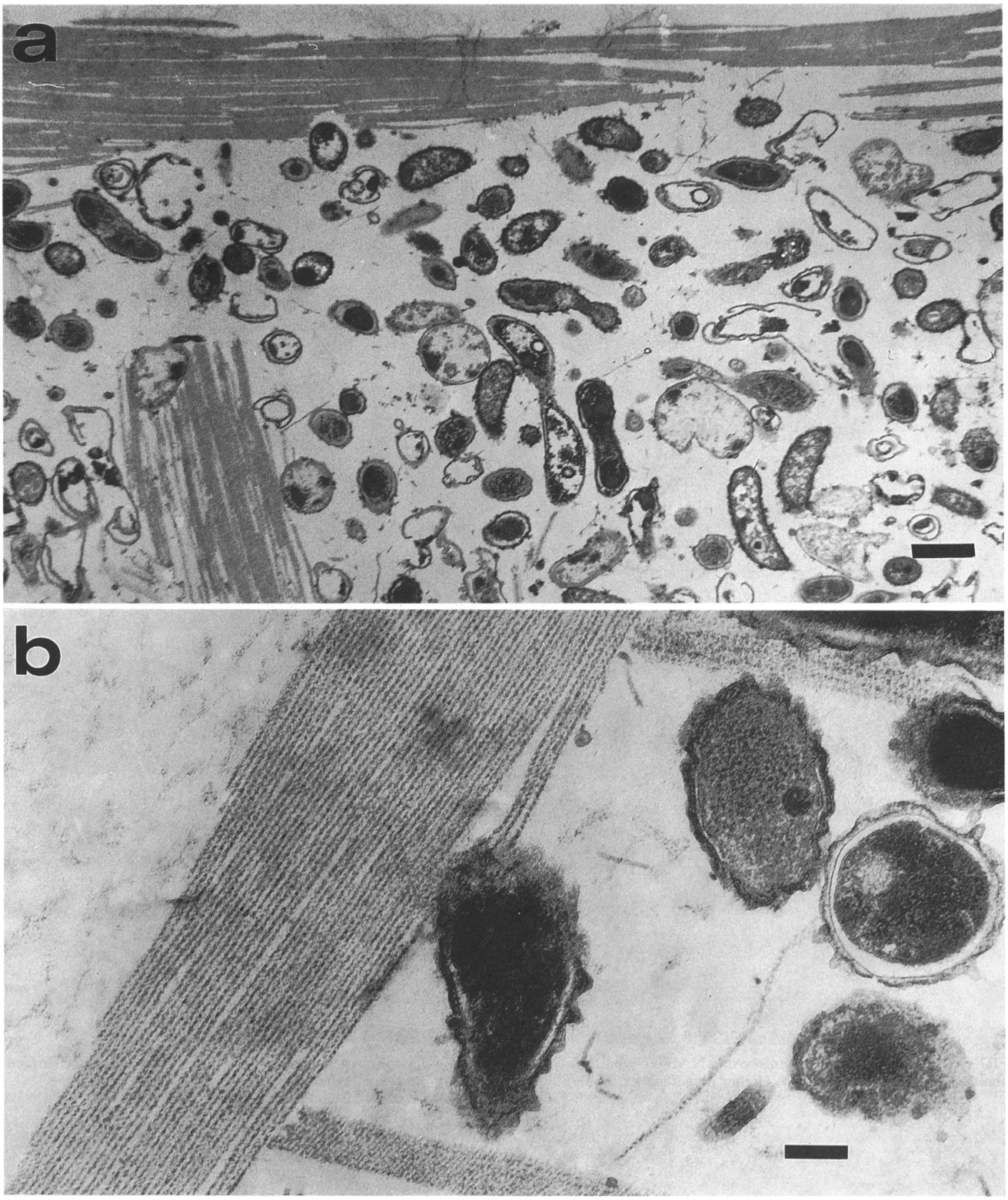

FIG. 8. Thin sectioning of colonies of *C. crescentus* CB15Ca10 grown on calcium-containing medium. (a) Low-magnification image of a cross-section through a colony. Note the layered stacks of darkly staining material; above the uppermost stack is the outside of the colony. (b) Higher-magnification image; note the absence of an S-layer on the cells. (c) High-magnification image of the layered stacks. Bars: 1 μm in panel a and 0.2 μm in panels b and c.

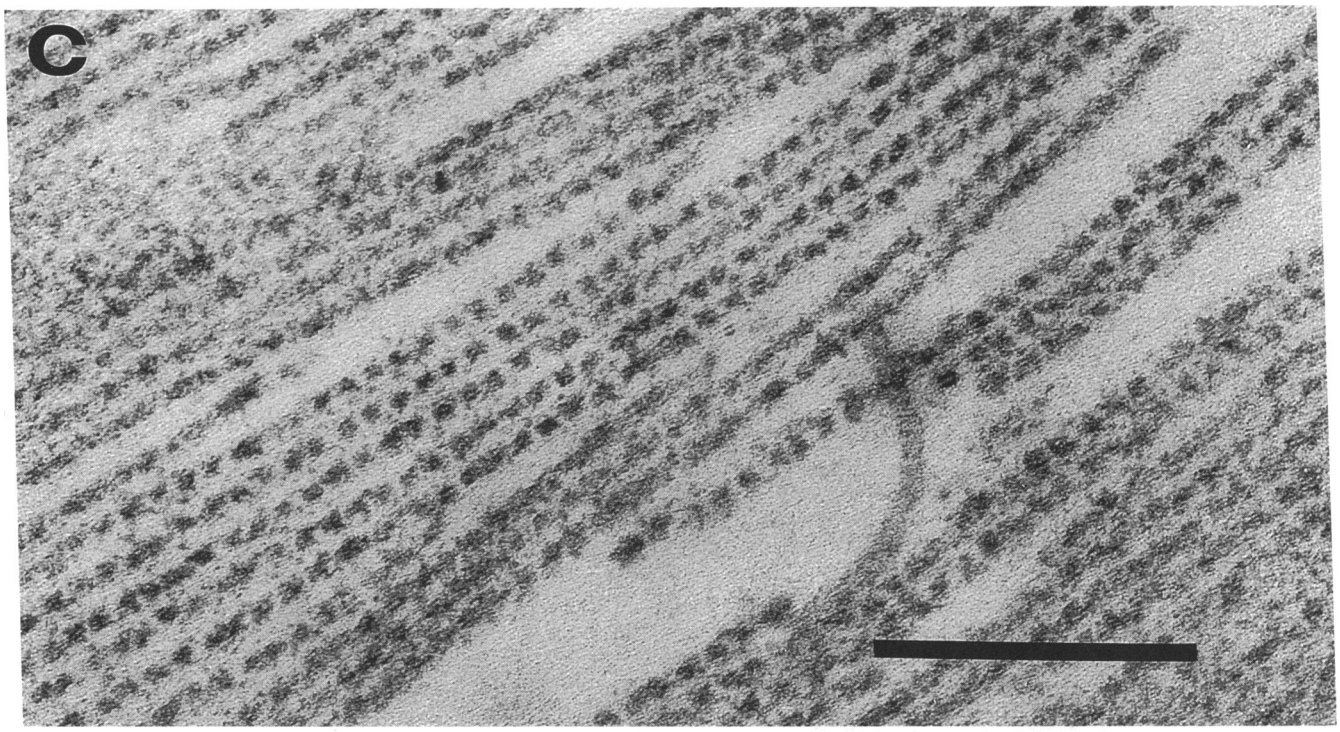

FIG. 8—*Continued.*

not yield values that lead to the assumption that the HPI layer is thicker (5.1 ± 0.5 nm [34]). If S-layers appear thinner in 3D reconstructions than expected from other investigations, flattening effects from adsorption or even conformational changes may be responsible. The latter was demonstrated for the S-layers of *Sporosarcina ureae* (11) and *A. vinelandii* (5).

Thin-section electron microscopy analysis of embedded colonies. Examination of embedded and thin-sectioned colonies of NA1000 (wild type with respect to the S-layer) yielded the expected results; the cells had a uniform S-layer attached to the surface of the outer membrane (Fig. 7), which is readily visible when fixation methods that incorporate tannic acid and ruthenium red are used (29). In contrast, S-layer-shedding mutant CB15Ca10 showed no indication of an S-layer on the cell surface (Fig. 8). Instead, extensive stacks of layered material were present in the colony, usually, although not always, near the upper surface of the colony; these showed center-to-center spacing of electron-dense regions that was comparable to the center-to-center spacing of the S-layer ring structures. It appeared as though the shed S-layer protein tended to migrate to the colony periphery and become incorporated into ever larger two-dimensional arrays. Presumably these large stacks break into smaller segments and intermix with cells during preparation for negative-stain electron microscopy. Interestingly, the stacks were composed of layers with a minimum thickness of approximately 20 nm, more than twice the thickness determined from the 3D reconstructions. Because of the flattening effects that occur in negative staining (as outlined above) and the dimensional changes that occur as a consequence of the thin-sectioning preparation process, including the use of tannic acid (29) during fixation and the plastic embedding process itself, it is difficult to make precise dimension comparisons between the two techniques. Even so, the thickness of the S-layer sheets noted in thin sections is best explained by the conclusion from image reconstructions that the S-layer fragments are mirror-image double layers.

When CB15Ca10 was grown on calcium-free medium, no S-layer was detected. Instead, a large amount of amorphous stained material was detected between cells, and the surface of most cells had an irregular amount of stainable material associated with the outer membrane, characteristics decidedly different from those of cells grown with calcium (Fig. 9). We hypothesize that without the ability to accumulate into S-layer structures, the exported RsaA protein still interacts weakly with the cell surface, leading to a loosely associated, unstructured protein layer.

Taken together, the observations from both image analysis and thin-section microscopy reinforce other data (9, 32, 33) suggesting that the RsaA protein attaches to the cell via calcium-mediated interactions with the outer membrane surface. In the absence of *C. crescentus* outer membrane material (or suitable sites in the membrane, in the case of the S-layer-shedding mutants), the development of an S-layer from RsaA still proceeds: the divalent character of calcium ions is used to bridge calcium interaction regions of the S-layer, forming a nearly perfect mirror image. This development apparently also occurs spontaneously when membrane material is disrupted by detergents, suggesting that, given the opportunity, an interaction with another sheet of the S-layer is thermodynamically preferred over attachment to membrane-derived molecules.

The findings also suggest, but do not prove, that calcium may be involved in the interaction between subunits, given the complete absence of organized structures under calcium-free conditions. Alternatively, it may be argued that the proper orientation of the RsaA molecule (by calcium-medi-

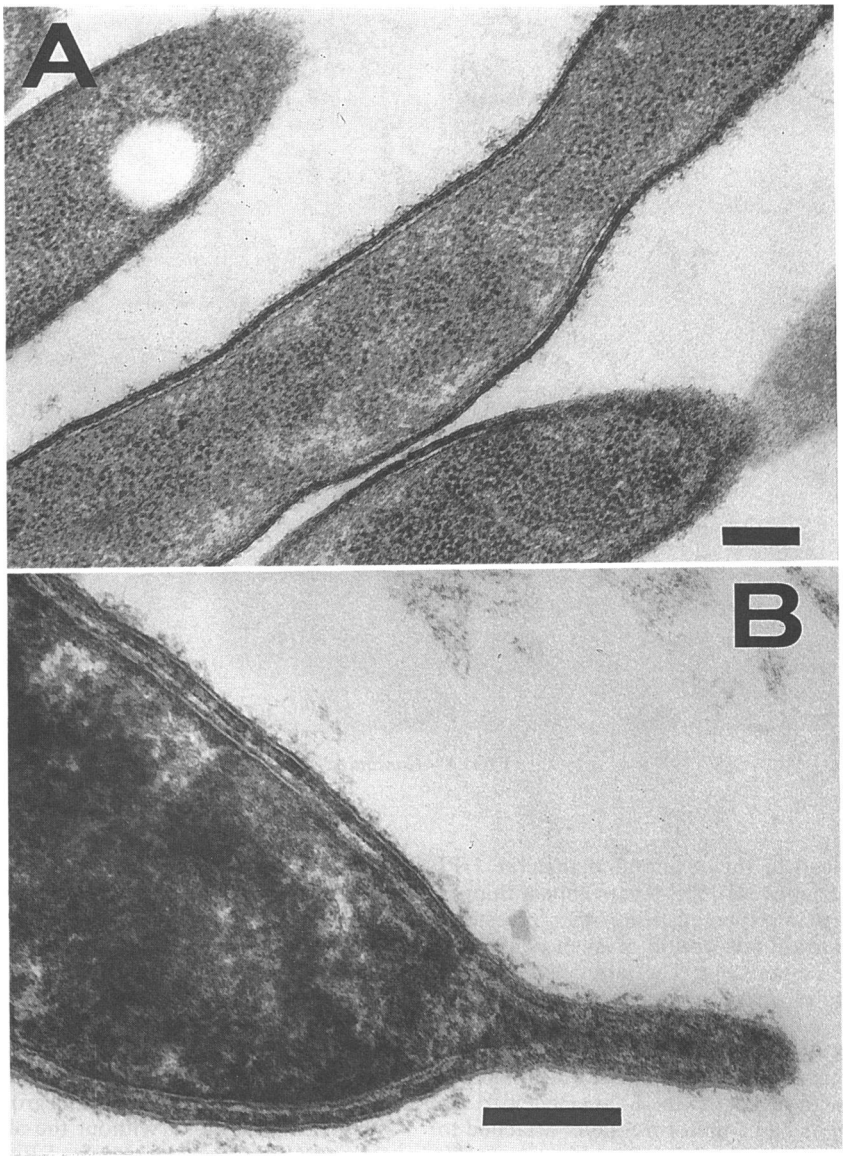

FIG. 9. Thin sectioning of *C. crescentus* CB15Ca10 cells grown on calcium-free medium. (A) Low-magnification image; note the presence of an irregular layer of stained material associated with most of the cell surface. (B) Higher-magnification image; no repeat structure can be discerned. Bars, 0.2 μm.

ated attachment to the outer membrane or another S-layer array) is essential for the efficient interaction of S-layer subunits. Assessing the specific role of regions of the gene hypothesized to be involved with calcium binding (13) should help resolve this issue.

The problems that occurred with the 3D reconstructions of the *C. crescentus* S-layer associated with attached lipid vesicles were not overcome with detergent-treated preparations. The incomplete staining of the relatively thick double layers and/or the dislocation from perfect alignment of the attached sheets, as well as possibly remaining lipid, are effects that are not desirable for reconstruction purposes. There was, however, another approach promising better preparations and reconstructions of the S-layer. As described earlier, strains CB15Ca5 and CB15Ca10 produce large and apparently lipid-free S-layer sheets that can be obtained with virtually no purification steps from colonies of cells grown on agar plates, similar to the procedure described for an *Aeromonas salmonicida* S-layer preparation (8). Two-dimensional reconstructions of the 0° tilt projection of these sheets showed that they were also double layered and, upon conventional negative staining, suffered from the same shortcomings for image reconstructions as detergent-treated preparations. However, initial experiments with ATG embedding yielded well-preserved, large, and uniformly stained S-layer sheets. The averages provided a significantly improved resolution of about 1.3 nm and a nearly perfect mirror-image symmetrical appearance of the projected structure (Fig. 10). These results were probably due to the complete embedding of the double layer in ATG, limiting or eliminating distortions that occur during specimen drying on the grid surface. The disadvantage of ATG as an embedding agent for electron microscopy is its sensitivity to decomposition in the electron beam, limiting the number of

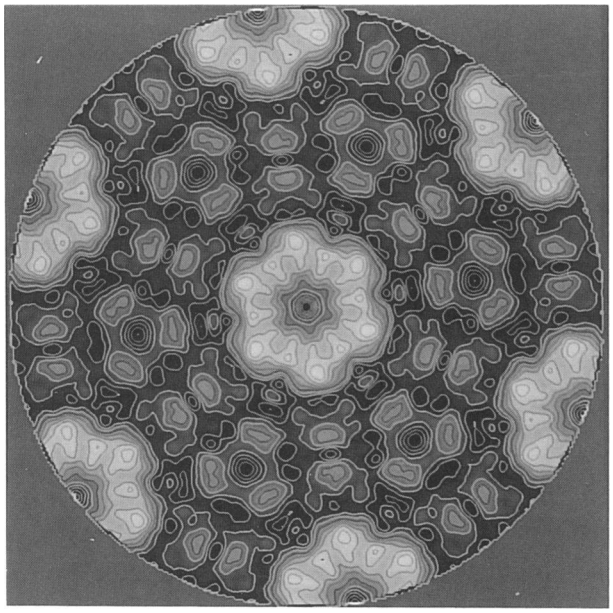

FIG. 10. Symmetrized correlation average of the S-layer obtained from the S-layer-shedding mutant CB15Ca10, embedded in ATG, and imaged under low-dose conditions. The sheet is double layered; therefore, the image is almost perfectly mirror symmetrical. The resolution is 1.3 nm (346 unit cells averaged). The lattice spacing is 21.8 nm.

micrographs that can be recorded in a tilt series. We are currently collecting data for a 3D reconstruction, merging the data from small tilt sets and estimating that we will achieve a resolution of about 1 nm, that should show further details of the structure of the *C. crescentus* S-layer.

ACKNOWLEDGMENTS

We thank Ute Santarius and Günter Pfeifer for skillful technical assistance.

This work was supported in part by grants to J.S. from the National Institutes of Health (GM-39055) and the Natural Sciences and Engineering Research Council of Canada (OGP0036574 and STR0118148).

REFERENCES

1. **Al-Karadaghi, S., D. N. Wang, and S. Hovmöller.** 1988. Three-dimensional structure of the crystalline surface layer from *Aeromonas hydrophila*. J. Ultrastruct. Mol. Struct. Res. **101:** 92–97.
2. **Baumeister, W., M. Barth, R. Hegerl, R. Guckenberger, M. Hahn, and W. O. Saxton.** 1986. Three-dimensional structure of the regular surface layer (HPI-layer) of *Deinococcus radiodurans*. J. Mol. Biol. **187:**241–253.
3. **Baumeister, W., I. Wildhaber, and B. M. Phipps.** 1989. Principles of organization in eubacterial and archaebacterial surface proteins. Can. J. Microbiol. **35:**215–227.
4. **Beveridge, T. J., and L. L. Graham.** 1991. Surface layers of bacteria. Microbiol. Rev. **55:**684–705.
5. **Bingle, W. H., H. Engelhardt, W. J. Page, and W. Baumeister.** 1987. Three-dimensional structure of the regular tetragonal surface layer of *Azotobacter vinelandii*. J. Bacteriol. **169:**5008–5015.
6. **Blaser, M. J., and E. C. Gotschlich.** 1990. Surface array protein of *Campylobacter fetus*: cloning and gene structure. J. Biol. Chem. **265:**14529–14535.
7. **Chu, S., S. Cavaignac, J. Feutrier, B. M. Phipps, M. Kostrzynska, W. W. Kay, and T. J. Trust.** 1991. Structure of the tetragonal surface virulence array protein and gene of *Aeromonas salmonicida*. J. Biol. Chem. **266:**15258–15265.
8. **Dooley, J. S. G., H. Engelhardt, W. Baumeister, W. W. Kay, and T. J. Trust.** 1989. Three-dimensional structure of an open form of the surface layer from the fish pathogen *Aeromonas salmonicida*. J. Bacteriol. **171:**190–197.
9. **Edwards, P., and J. Smit.** 1991. A transducing bacteriophage for *Caulobacter crescentus* uses the paracrystalline surface layer protein as a receptor. J. Bacteriol. **173:**5568–5572.
10. **Engelhardt, H.** 1988. Correlation averaging and 3-D reconstruction of 2-D crystalline membranes and macromolecules, p. 357–413. *In* F. Mayer (ed.), Methods in microbiology, vol. 20. Academic Press, London.
11. **Engelhardt, H.** 1991. Electron microscopy of microbial cell wall proteins. Surface topography, three-dimensional reconstruction, and strategies for two-dimensional crystallization, p. 11–25. *In* J. P. Latgé and D. Boucias (ed.), Fungal cell wall and immune response. NATO ASI series H53. Springer-Verlag KG, Berlin.
12. **Fisher, J. A., J. Smit, and N. Agabian.** 1988. Transcriptional analysis of the major surface array gene of *Caulobacter crescentus*. J. Bacteriol. **170:**4706–4713.
13. **Gilchrist, A., J. A. Fisher, and J. Smit.** 1992. Nucleotide sequence analysis of the gene encoding the *Caulobacter crescentus* paracrystalline surface layer protein. Can. J. Microbiol. **38:**193–202.
14. **Hovmöller, S., A. Sjögren, and D. N. Wang.** 1988. The structure of crystalline bacterial surface layers. Prog. Biophys. Mol. Biol. **51:**131–163.

14a. **Jakubowski, U., R. Hegerl, H. Formanek, S. Volker, U. Santarius, and W. Baumeister.** Unpublished results.

15. **Kay, W. W., B. M. Phipps, R. A. Garduño, and T. J. Trust.** 1988. The A-layer of *Aeromonas salmonicida*: organization and functions, p. 44–50. *In* U. B. Sleytr, P. Messner, D. Pum, and M. Sara (ed.), Crystalline bacterial cell surface layers. Springer-Verlag KG, Berlin.
16. **Koval, S. F., and S. H. Hynes.** 1991. Effect of paracrystalline protein surface layers on predation by *Bdellovibrio bacteriovorus*. J. Bacteriol. **173:**2244–2249.
17. **Peters, J., M. Peters, F. Lottspeich, and W. Baumeister.** 1989. S-layer protein gene of *Acetogenium kivui*: cloning and expression in *Escherichia coli* and determination of the nucleotide sequence. J. Bacteriol. **171:**6307–6315.
18. **Peters, J., M. Peters, F. Lottspeich, W. Schäfer, and W. Baumeister.** 1987. Nucleotide sequence analysis of the gene encoding the *Deinococcus radiodurans* surface protein, derived amino acid sequence, and complementary protein chemical studies. J. Bacteriol. **169:**5216–5223.
19. **Poindexter, J. S.** 1964. Biological properties and classification of the *Caulobacter* group. Bacteriol. Rev. **28:**231–295.
20. **Poindexter, J. S.** 1978. Selection for nonbuoyant morphological mutants of *Caulobacter crescentus*. J. Bacteriol. **135:**1141–1145.
21. **Rachel, R., J. Jakubowski, H. Tietz, R. Hegerl, and W. Baumeister.** 1986. Projected structure of the surface protein of *Deinococcus radiodurans* determined to 8 Å resolution by cryomicroscopy. Ultramicroscopy **20:**305–316.
22. **Saxton, W. O., and W. Baumeister.** 1982. The correlation averaging of a regularly arranged bacterial cell envelope protein. J. Microsc. (Oxford) **127:**127–138.
23. **Saxton, W. O., and W. Baumeister.** 1986. Principles of organization in S-layers. J. Mol. Biol. **187:**251–253.
24. **Saxton, W. O., W. Baumeister, and M. Hahn.** 1984. Three-dimensional reconstruction of imperfect two-dimensional crystals. Ultramicroscopy **13:**57–70.

24a. **Saxton, W. O., I. J. Pitt, and M. Horner.** 1979. Digital image processing: the SEMPER system. Ultramicroscopy **4:**343–354.

25. **Sleytr, U. B., and P. Messner.** 1988. Crystalline surface layers in procaryotes. J. Bacteriol. **170:**2891–2897.
26. **Smit, J.** 1986. Protein surface layers of bacteria, p. 343–376. *In* M. Inouye (ed.), Bacterial outer membranes as model systems. John Wiley & Sons, Inc., New York.
27. **Smit, J., and N. Agabian.** 1982. Cell surface patterning and morphogenesis: biogenesis of a periodic surface array during

Caulobacter development. J. Cell Biol. **95:**41–49.
28. **Smit, J., and N. Agabian.** 1984. Cloning of the major protein of the *Caulobacter crescentus* periodic surface layer: detection and characterization of the cloned peptide by protein expression assays. J. Bacteriol. **160:**1137–1145.
29. **Smit, J., D. A. Grano, R. M. Glaeser, and N. Agabian.** 1981. Periodic surface array in *Caulobacter crescentus*: fine structure and chemical analysis. J. Bacteriol. **146:**1135–1150.
30. **Tsuboi, A., R. Uchihi, T. Adachi, T. Sasaki, S. Hayakawa, H. Yamagata, N. Tsukagoshi, and S. Udaka.** 1988. Characterization of the genes for the hexagonally arranged surface layer proteins in protein-producing *Bacillus brevis* 47: complete nucleotide sequence of the middle wall protein gene. J. Bacteriol. **170:**935–945.
31. **Tsuboi, A., R. Uchihi, R. Tabata, Y. Takahashi, H. Hashiba, T. Sasaki, H. Yamagata, N. Tsukagoshi, and S. Udaka.** 1986. Characterization of the genes coding for two major cell wall proteins from protein-producing *Bacillus brevis* 47: complete nucleotide sequence of the outer wall protein gene. J. Bacteriol. **168:**365–373.
32. **Walker, S. G., N. Ravenscroft, and J. Smit.** Unpublished data.
33. **Walker, S. G., S. H. Smith, and J. Smit.** 1992. Isolation and comparison of the paracrystalline surface layer proteins of freshwater caulobacters. J. Bacteriol. **174:**1783–1792.
34. **Wang, Z., T. Hartmann, W. Baumeister, and R. Guckenberger.** 1990. Thickness determination of biological samples with a z-calibrated scanning tunneling microscope. Proc. Natl. Acad. Sci. USA **87:**9343–9347.